Conf-940399--2

LA-UR 94-4374

Title: ISSUES RELATED TO PREDICTION OF RESIDUAL STRESSES IN TITANIUM ALLOY MATRIX COMPOSITES

Author(s): P. Rangaswamy, N. Jayaraman

Submitted to: ASTM Symposium: "Life Prediction Methodology for Titanium Matrix Composites," Hilton Head Island, SC, 22-24 March 1994

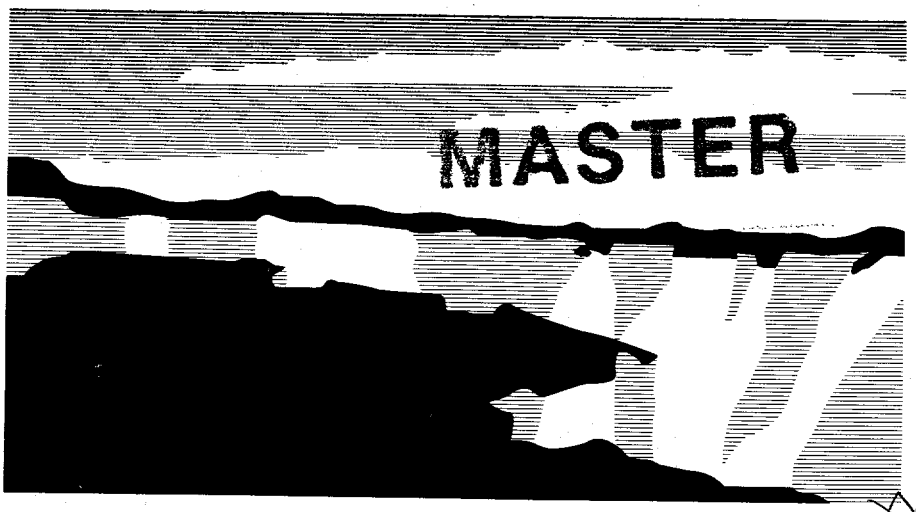

Los Alamos
NATIONAL LABORATORY

Form No. 836 R5
ST 2629 10/91

ASTM Symposium on "Life Prediction Methodology for Titanium Matrix Composites", presented at Hilton Head Island, SC, USA, 22-24 Mar. 1994

ISSUES RELATED TO PREDICTION OF RESIDUAL STRESSES IN TITANIUM ALLOY MATRIX COMPOSITES

Partha Rangaswamy
LANSCE/MST-5, Los Alamos National Laboratory, Los Alamos New Mexico 87545

N. Jayaraman
Department of Materials Science and Engineering
University of Cincinnati, Cincinnati, OH 45221-0012
Telephone: (513) 556-3112

ABSTRACT:

Recently, a detailed study of residual stresses on the as-processed SCS-6/Ti-24Al-11Nb $[0]_8$ composite, and SCS-6/Beta-21S composites in uni-directional $[0]_4$, cross-ply $[0/90]_s$, and quasi-isotropic $[0/\pm45/90]_s$ lay-ups has been completed. In this study, residual stresses have been measured using x-ray diffraction ($Sin^2\psi$) technique. We have shown that the use of conventional unit cell models consisting of a quarter fiber surrounded by the matrix material to predict residual stresses for verification of experimental results is inadequate. Such models have successfully predicted the stresses at the fiber-matrix interface. However, experimental work to measure residual stresses have always been on surfaces far away from the interface region.

In this paper, the approach taken in extending the conventional unit cell model to the concept of multi-fiber models to predict average stresses are presented. In this process, several modeling issues have been identified. These issues are (i) use of conventional unit models for prediction of average surface residual stresses, (ii) effect of orientation of the sub-surface plies on the residual stresses in the surface ply, (iii) residual stresses in the interior plies, and (iv) constituent material properties.

KEY WORDS: residual stress, finite element models (FEM), material removal effects, metal matrix composites (MMCs), X-ray stress measurements, titanium matrix, composites, coefficient of thermal expansion (CTE) mismatch.

1. Residual Stresses in Metal Matrix Composites:

It is well known that the origin of residual stresses in as-processed Metal Matrix Composites are due to the Coefficient of Thermal Expansion (CTE) mismatch between the reinforcement and the matrix material and the temperatures used in the processing of these composites. Other factors such as fiber orientation in a ply and stacking arrangement of these plies could also affect the nature and distribution of these stresses. Finally one also has to take into account the basic constituent properties of the metal matrix and the reinforcement which could generally vary with temperature. The elastic-plastic behavior of the constituents, for example, may even exhibit time-temperature dependence. Also, one has to recognize the role of material properties and particularly, the fact that some of the constituent properties are sensitive to processing conditions and corresponding microstructural conditions. This is particularly true of those titanium alloy matrix materials that show potential to develop textures and therefore anisotropic properties. All the above factors could lead to a complex residual thermal stress-strain state both during processing and during service at elevated temperatures.

Residual stresses are generally measured on the surface of the metal matrix composite material using non-destructive techniques such as x-ray diffraction, neutron diffraction etc. [1-15]. In many of these techniques, stress measurements are made by using a beam of finite size, which covers several fiber diameters on the surface of a sheet specimen (Fig. 1). Generally, x-rays have very limited depth-of-penetration in metal specimens (less than about 10 microns). Therefore, the stresses measured are an average of all the stress gradients seen in the measuring direction in the specimen within the beam exposed volume. Residual stress measurements have been generally made in the direction of fiber (Longitudinal stress, σ_L), transverse to the direction of fiber (Transverse stress, σ_T) and at any other angle to the fiber (σ_ϕ) [2-10]. The stress profiles of the measured values are obtained by successive electropolishing of surface layers. Attempts have been made to verify these results using conventional concentric cylinder model and finite element solution for a unit cell model (Fig. 2) [12-26]. Under these conditions the normally used procedures of comparing the average stresses measured on the surface and the stress profiles obtained from electropolishing using x-ray diffraction technique with the CCM or UCM models are inadequate. The number and orientation of sub-surface plies also have to be taken into consideration when predicting these stress profiles.

Recently, we have completed a detailed study of residual stresses on the as-processed SCS-6/Ti-24Al-11Nb $[0]_8$ composite, and SCS-6/Beta-21S composites in uni-directional $[0]_4$, cross-ply $[0/90]_s$, and quasi-isotropic $[0/\pm45/90]_s$ lay-ups. The x-ray measurements were made in three different orientations on both surfaces of the composite: parallel (σ_L), transverse (σ_T) and 45° (σ_{45}) to the fiber direction as shown in Fig. 1. In this study we used a beam size of about 3mm by 7mm for $\psi = 0^\circ$ and 6 mm by 7 mm for $\psi = 60^\circ$. The relatively large size of the beam encompasses an area covering at least 15 to 20 fibers which measures an average diameter of 140 microns each. Profiles of these average stress values vs. depth (i.e. after removing layers by electropolishing) from both surfaces of the as-received plate are shown in Fig. 8. To compare with the experimental results, finite element models were developed and designed to simulate real experimental conditions where the average stresses can be calculated with little or no interference from the imposed surface boundary conditions in the conventional concentric cylinder models (CCM) or the unit cell models (UCM) as also shown in Fig. 8. These results will be explained in detail in the later sections of this paper.

In this process, several modeling issues have been identified. These issues are (i) use of conventional unit models for prediction of average surface residual stresses, (ii) effect of orientation of the sub-surface plies on the residual stresses in the surface ply, (iii) residual stresses in the interior plies, and (iv) material properties.

2. Prediction of surface residual stresses in a unidirectional MMC:

The initial approach taken in developing the finite element models was based on first developing the UCM (Fig. 2), and adding to it additional fibers taking advantage of the symmetry boundary conditions offered by the finite element modeling technique. By choosing this approach we could compare the stress prediction in the surface layers of the unit cell model and the multi-fiber models with the experimental results for verification. Without going into the details of the analysis which has been exhaustively explained in references 5 and 20 it was found that beyond the one fiber model (Figs. 3 and 4), development of the additional models such as two fiber, three fiber etc., proved to give the same results of the one fiber model because the additional models were repetition of the one fiber model and therefore similar results had to be expected. From these results the one fiber model was essentially representative of a two ply model. Therefore the one fiber model henceforth would also be called a two ply model. The two ply model was extended to develop four ply and eight ply models of a uni-directional MMC (Figs. 3 - 5). The surface region of the models have been divided into layers to simulate material removal. Without going into the details of model development, codes, thermal loading procedure, boundary conditions, layer removal technique which has been explained in previous papers by the authors [5,6,20], we will however briefly explain the finite element modeling procedure used in these analysis.

Boundary Conditions

All the models were analyzed under symmetry boundary conditions on three mutually perpendicular faces and two out of the other three surfaces were subjected to generalized plane strain (constant strain) conditions, and the third surface (the top surface) was constraint free. These boundary conditions are shown schematically in Fig. 3. Because of symmetry in the boundary conditions, a one quarter fiber model ($\frac{1}{4}$x1) actually predicts residual stress for a one fiber model (single ply). Similarly, a one fiber model (1x1) predicts residual stress for four fibers (two plies, i.e. two fibers in the top and bottom ply respectively), and the two fiber model (2x1) predicts residual stress for eight fibers (two ply also, but four fibers in the top and bottom plies respectively) etc.

Thermal Loading Procedure

In this study, only development of thermal residual stresses have been considered. The stresses are assumed to be zero at a temperature of 950° C for this composite. Since the matrix material has low modulus, very low strength, and high ductility at temperatures in the neighborhood of the assumed processing temperature, the choice of the exact processing temperature is not very critical to the final solution. Residual stresses in the fiber alone due to its own manufacturing process, if any, were ignored. **NIKE3D** (Non-linear structural finite element code) [27] used to perform the finite element analysis uses a modified Newton-Raphson stiffness formulation to solve the non-linear equations. The thermal loading curve is divided into a number of increments and an iterative solution performed at each increment. The stiffness matrix is reformed at each increment. Small displacement theory is used. The plasticity algorithm makes use of a Von Mises yield surface model with associated plastic flow. Isotropic hardening was assumed in this analysis.

The initial analysis of residual stress was performed by dividing the cooling process into 100 steps for a total time of 1000 seconds. The FEM code has an option of incrementing through an auto time step-size control or fixed time step-size control. The choosing of either option did not however have any significant effect on the results. About three to four iterations were generally required to obtain convergence at each time step.

Layer Removal Technique

In the experimental study as described in reference [2-4, 20] residual stress profiles in composite plates was measured by removing thin layers of matrix material. Material removal was done symmetrically on both sides of the composite plate, in order to avoid inducing any bending effects. To simulate the material removal sequence, the surface regions of the composite models were modeled as layers. For example, Figs. 2, 4 and 5 show the surface regions of the matrix material arranged in the form of layers.

The removal of material is simulated by using the element birth/death option built in the finite element code or by identifying each layer of elements with different material identifier codes and deleting these materials in the re-start procedure used after thermal loading of the composite to ambient temperature. The theory of material removal simulation by using the birth/death option in the finite element analysis code and examples of using this option to verify results of solutions obtained through analytical methods are explained in the Appendix of reference 5.

Fig. 7 shows the variation in the average stresses upon material removal in the longitudinal direction (fiber direction) and transverse direction for the UCM, two-ply, four-ply and eight-ply models for the SCS-6/Ti-24Al-11Nb $[0]_8$ composite. Average stresses on the surface of the composite for all the components were computed by taking the average of individual elemental stress values on the outer surface. Such stress averaging was accomplished by using the Simpson's rule, a well established numerical integration procedure. Before material removal, the average stresses predicted in the surface layer are the same for all the four models. This is indeed true (not shown) for all the layers in these models. But upon layer removal the changes in stresses are highest in the unit-cell model and the least in the eight-ply model. The longitudinal stresses in the layer closest to the fiber-matrix interface for the unit-cell, two-ply, four-ply and eight-ply models are 396, 328, 316 and 302 MPa respectively. Similarly the transverse stresses in the layer closest to the fiber-matrix interface for the unit-cell, two-ply, four-ply and eight-ply models are 214, 111, 107 and 91 MPa respectively. These changes show the influence of the underlying fibers on the overall distribution of residual stresses in the composite. All these differences between the four models can be explained on the basis of volume fraction effects: that is, the differences are essentially due to different amounts of matrix material being removed in an otherwise apparently similar layer removal process used in all these models. In comparing the unit cell model and the two-ply model, due to the location of symmetric boundaries, twice the amount of material is removed and therefore these lead to a greater change in adjustment of residual stresses in the unit-cell model. This reasoning can be extended to the four-ply and eight-ply models also. For the removal of an equivalent layer in the two-ply model, the increase in volume fraction will be greater as compared to the four-ply or the eight-ply model. In other words, the greater the change in volume fraction of the matrix, the greater will be the change in the residual stress. The results in Fig. 7 support this analysis. The predicted results from the FEM models above have been compared with experimental results and are shown in Fig. 8. In general as shown in the figure the experimental results compare more favorably with the FEM results of the eight-ply (multi-ply) models than the conventional unit cell model. Similar observations have been made for the SCS-6/Beta21S $[0]_4$ composite. Conventionally, the unit cell model is used for most FEM analysis. The issue here clearly demonstrates the inadequacy of the

conventional UCM to predict the changes in the residual stresses due to layer removal to obtain stress profile

3. Effect of stacking ply orientation on the surface residual stresses:

It has been shown thus far, that the underplies in a unidirectional composite have an effect on the surface residual stress distribution after the layer removal process. If indeed this is true, then the analysis of a cross-ply $[0/90]_s$ (Fig. 9), and a angle ply $[0/45]_s$ model (Fig. 10), would also show an influence of the under plies on the stress/strain states on the surface of the composite.

The results for the longitudinal stresses and transverse stresses in the matrix material for a SCS-6/Beta-21S four-ply $[0]_4$ composite and the cross-ply $[0/90]_s$ models are shown in Figs. 11 A and 11 B. The differences in the residual stress states between the unidirectional and the cross-ply composite are clearly contrasted in the residual stress plots for the longitudinal and transverse stresses. As seen in these figures, while the longitudinal and transverse stresses show similar trends for the cross-ply composite (Fig. 11 B), these stresses are significantly different in the unidirectional composite (Fig. 11 A). This difference between the two ply lay-ups indicates the strong influence of the underlying plies on the stress/strain states of the surface ply.

Results of the finite element models are compared with experimental results in Figs. 12 A and 12 B for the unidirectional and cross-ply composites, respectively. In these figures, the average longitudinal ($<\sigma_L>$), and transverse stresses ($<\sigma_T>$) from the finite element models after the layer-removal process and the residual stresses in the longitudinal (σ_L) and transverse (σ_T) directions obtained from experiments are plotted as a function of distance above the fibers. Figs. 12 A and 12 B show very favorable comparisons in the trends in the variation of experimental and predicted residual stress profiles.

4. Residual stresses in internal ply:

Residual stress analysis in the internal (second) ply was conducted by removing symmetrically the surface ply (both matrix and the fiber layer) on both top and bottom surfaces of the model. This was done to simulate the corresponding experimental residual stress analysis conducted using x-ray diffraction technique [3,4,6,20]. Finite element prediction of residual stresses in the internal (second) ply for the eight-ply model was analyzed and the results are shown in Fig. 13. The longitudinal, transverse and out-of-plane (σ_Z) stresses as a function of distance above the fiber plane are shown in this Fig. 13. The average residual stresses in the surface-ply in the longitudinal and transverse directions are higher than the corresponding stresses in the second-ply. The average out-of-plane stresses (σ_Z) in the surface-ply are consistently close to zero implying plane stress conditions. However, in the second-ply, the average σ_Z is gradually increasing from the outer surface layer towards the fiber-matrix interface layer. The fact that the σ_Z, which is the average elemental stress in the out-of-plane direction is not zero, implies that the σ_Z gradient is very steep. The reasons for the steep stress gradient in the out-of-plane direction are indication of the severity of the tri-axial stress state developed in the region between the two fiber plies. The FEM results seem to support the experimental observations.

In the measurement of residual stresses using the x-ray diffraction technique, normally one would expect for a biaxial plane stress condition on the surface, the $d_{\phi\psi}$ vs.

$Sin^2\psi$ plot to be linear (where $d_{\phi\psi}$ is the average interplanar spacing of the crystallographic planes, and ϕ and ψ are specimen orientation parameters [20]). Any non-linearity in this plot is normally attributed to severe stress gradients in the sampling volume and possible contribution from out-of-plane (σ_Z) stresses. Indeed, this was observed as shown in Fig. 13. In fact, to further prove this point, using the FEM results, the $d_{\phi\psi}$ vs. $Sin^2\psi$ was predicted for the second ply and a favorable comparison was seen between the predicted and experimentally observed plots, as seen in Figs. 14 A and B.

5. Influence of material properties on residual stresses in MMCs:

The material properties used in the finite element models are assumed isotropic and the constitutive behavior of the matrix material to be thermal elastic/plastic and the fiber to be thermal elastic. For this type of material model behavior, the constitutive material properties which are used are the Young's Modulus (E_m), Plastic Modulus (E_p), Poisson's Ratio (ν), Yield Strength (σ_y), and Thermal Coefficient Expansion (α) which are temperature dependent. Even though a more rigorous analysis would consider, thermal elastic/plastic/creep behavior of the matrix material, more sophisticated material models including creep effects were not considered mainly due to the fact that other researchers found the effect of creep to be insignificant on residual stresses in these materials [12-19, 22-26].

For the SCS-6/Ti-24Al-11Nb and SCS-6/Beta-21S material systems used in this study, the influence of these constitutive material properties on the state of residual stresses could throw some light on the overall stress distribution. In comparing the residual stress profiles in the as-cooled and the material removal conditions for a two-ply model it does appear for the same volume fraction and temperature of processing the mis-match in the thermal coefficient of expansion plays a more significant role in the stress distribution, than the constituent properties such as Yield Strength, Elastic Modulus, Plastic Modulus and Poisson's Ratio, although, referring to Table 1 the material properties for the two matrices show major differences in Yield Strength, Elastic Modulus, Plastic Modulus and Thermal Coefficient of Expansion. Also, for a simple one dimensional problem assuming thermal elastic behavior the longitudinal stresses in the matrix and fiber along the direction of the fiber axis under iso-strain conditions are

$$\sigma_m = \frac{V_f E_m E_f \Delta\alpha \Delta T}{E_c} \qquad [1]$$

$$\sigma_f = -\frac{V_m E_m E_f \Delta\alpha \Delta T}{E_c} \qquad [2]$$

assuming $\Delta\alpha = \alpha_m - \alpha_f$ and $\Delta T = T_{high} - T_{low}$
where the key variables that directly influence the magnitude of the residual stresses are the CTE mismatch ($\Delta\alpha$), the fiber volume fraction (V_f) and the temperature change (ΔT) [20].

Substituting the appropriate material properties from Table 1 for the two matrix materials, it turns out that the matrix stresses for the Ti-24Al-11Nb and Beta-21S matrix systems are 369 MPa and 350 MPa respectively, using equation 1. The finite element results from Table 2 show an average longitudinal stress of 292 MPa and 283 MPa for Ti-24Al-11Nb and Beta-21S matrix material respectively. The differences between the two material systems seem to be in fair agreement with the simple one dimensional analytical model, considering that the constitutive model used in the finite element model is thermo-elastic-plastic behavior of the matrix material and the material properties used are

temperature dependent. Therefore the slight increase in stresses in the Ti-24Al-11Nb matrix composite as compared to the Beta-21S matrix composite clearly underlines the impact of the mismatch in the thermal coefficients of the matrix phase and reinforcement phases for the same volume fraction and temperature change.

It is also interesting to note that the lower yield strength, and Young's modulus of the Ti-24Al-11Nb matrix material could have contributed to the dropping of the transverse stresses because the Von Mises effective stresses approaches the yield strength of the matrix material (Table 2), whereas the higher yield strength and Young's modulus of the Beta-21S matrix material has not caused any change in the longitudinal and transverse stresses because the effective stresses are comparatively small compared to the yield strength of the matrix material (Table 2). The transverse stresses in the layers close to the fiber are also strongly influenced by the hoop stresses which approaches a maximum close to the fiber-matrix interface. Interestingly, this also explains why the stresses in the second ply region are lower than the surface ply regions. This is because of the increase in plastic deformation which is controlled by the Von Mises yield criteria in the FEM technique due to the presence of the tri-axial state of stresses in the second ply region influenced by the presence of the two fibers, whereas in the surface ply the tri-axial stress exists very close to just one fiber.

6. Summary:

It is evident from this work that close attention should be paid to the experimental methods used in measurement and the models used for prediction of residual stresses in MMCs. Specifically, prediction models should be designed to simulate real experimental conditions. Many of the reported residual stress measurements in MMCs are done by the conventional x-ray diffraction technique. The stress profiles are usually obtained by successive electropolishing of surface layers. Under these conditions, it is shown here that the conventional unit cell models are inadequate to predict the stress profiles resulting from the electropolishing. The number and orientation of sub-surface plies have been shown to play a significant role on the residual stress profile of the surface ply.

7. Acknowledgments:

The authors wish to thank the Ohio Super Computer Center (Steve Koehl and Larry Cooper) for a grant (PES 454) for running the LLNL codes. The authors also wish to thank Robert Whirley of LLNL for helpful discussions on the codes and the personnel from WL/MLLN for their support, particularly Ted Nicholas, Jim Larsen and Noel Ashbaugh. Many helpful discussions with Ken Wright of General Electric are also gratefully acknowledged.

8. References:

1. S. Tsai, D. Mahulikar and H.L. Marcus: Materials Science and Engineering, 1981, 47 pp. 145-149.

2. P. Rangaswamy, W.C. Revelos and N. Jayaraman: *"A Study of residual stresses in SCS-6/Ti-24Al-11Nb Metal Matrix Composite"*, Published in Residual Stresses in Composites: Measurement, Modeling and Thermo-mechanical Modeling, ed. E. V. Barrera and I. Dutta, TMS. Proceedings 122nd TMS Annual Meeting, Feb. 21-25, 1993, Denver, CO.

3. N. Jayaraman and P. Rangaswamy: *"Residual Stresses in Ti3Al-SCS-6 Fiber Reinforced Metal Matrix Composites"*, in Proceedings from Titanium Aluminide

Composite Workshop, eds. P.R. Smith, S.J. Balsone and T. Nicholas, WL-TR-91-4020, Materials Behavior Branch, Wright Laboratory, WPAFP (1991).

4. P. Rangaswamy, W.C. Revelos and N. Jayaraman: *"Residual stresses in SCS-6/Ti-24Al-11Nb Composite: Part 1- Experimental"*; Journal of Composites and Technology Research, (JCTRER), Vol. 16, No. 1, January 1994, pp. 47-53.
5. P. Rangaswamy, and N. Jayaraman: *"Residual Stresses in SCS-6/Ti-24Al-11Nb Composite: Part II - Finite Element Modeling"*, Journal of Composites and Technology Research, (JCTRER), Vol. 16, No. 1, Janauary 1994, pp. 54-67.
6. P. Rangaswamy, and N. Jayaraman, *"Residual stresses in SCS-6/Beta-21S Metal Matrix Composites"*, Accepted and to be published in Journal of Composites and Technology Research, (JCTRER).
7. B.N. Cox, M.R. James, D.B. Marshall, and R.C. Addison, Jr: Metallurgical Transactions A, 1990, Vol. 21 A, pp 2701.
8. M.R. James, *"Behavior of Residual Stresses during Fatigue of Metal Matrix Composites"*, Residual Stresses-3, ed. H. Fujiwara, T. Abe and K. Tanaka, Elsevier, pp 555-560 (1992).
9. M.R. James, M.A. Bourke, J.A. Goldstone and A.C. Lawson: "Residual Stress Measurements in Continuous Fiber Titanium Matrix Composites", Advances in X-Ray Analysis, Vol. 36., (1993) in press.
10. M.R. James, "Residual Stresses in Metal Matrix Composites", International Conference on Residual Stresses II. eds. G. Beck, S. Denis and A. Simon, Elsevier, pp. 429-35 (1989).
11. K.M. Brown, R.W. Hendricks, and W.D. Brewer: "X-Ray Diffraction Measurements of Residual Stresses in SiC/Ti Composites", TMS Fall Meeting, Indianapolis, Indiana, October 1-5, 1989.
12. P.K. Wright, M.D. Sensmeier, D. Kupperman and H. Wadley: "Thermal stress effects in intermetallic matrix composites", NASA Contract No. NAS3-25790, Lewis Research Center, Cleveland, OH, 1991, Report No. 21.
13. A. Saigal, D.S. Kupperman and S. Majumdar: Materials Science and Engineering, 1992, AI50, pp. 59-66.
14. S. Majumdar, J.P. Singh, D. Kupperman and A.D. Krawitz, Application of Neutron Diffraction to Measure Residual Strains in Various Engineering Composite Materials, J. Eng. Mat. and Tech., 113:51-59 (1991).
15. D.S. Kupperman, S. Majumdar, J.P. Singh, Residual Strain in Adavanced Composites, Neutron News, 2:15-18 (1991).
16. N. Ashbaugh, M. Khobaib, R. John, et al: "Mechanical Properties of Advanced Engine Materials", Final Report, Air Force Contract WL-TR-91-4149; Wright-Patterson Air Force Base, OH (April 1992).
17. W.S. Johnson, S.J. Lubowinski, and A.L. Highsmith: Thermal and Mechanical Behavior of Ceramic and Metal Matrix Composites, ASTM STP 1080, J.M. Kennedy, H.H. Moeller, and W.S. Johnson, Eds. Philadelphia, 1990, pp. 193-218.
18. C.A. Bigelow, W.S. Johnson and A.R. Naik: "A comparison of various micromechanics models for metal matrix composites", Mechanics of Composite Materials and Structures. Eds: J.N. Reddy and J.L. Telpy, 1989.
19. C. Bigelow: "Thermal residual stresses in a Silicon-Carbide/Titanium [0/90] Laminate", Submitted to Journal of Composites and Technology Research, July 1992.
20. Partha Rangaswamy: A Study of Residual Stresses in Titanium Metal Matrix Composites, Ph.D Thesis, University of Cincinnati, 1992-1993.
21. M. Uemura, H. Iyama. and Yamaguchi: Journal of Thermal Stress, 1979, Vol.2, pp. 393 - 412.
22. M. Vedula, R.N. Pangborn and R.A. Queeney: Composites, 1988, 19 No. 1, pp 55-60.

23. M. Vedula, R.N. Pangborn and R.A. Queeney: Composites, 1988, 19 No. 2, pp 55-60.
24. M.R. Wisnom: Journal of Composite Materials, 1990, No. 24, pp 707-727.
25. R. P. Nimmer: Journal of Composites Technology & Research, 1990, Vol. 12, No. 2, pp. 65-75.
26. J.L. Kroupa: "Elastic-Plastic FEM analysis of MMC subjected to Thermomechanical Fatigue", in Proceedings from Titanium Aluminide Composite Workshop, eds. P.R. Smith, S.J. Balsone and T. Nicholas, WL-TR-91-4020, Materials Behavior Branch, Wright Laboratory, WPAFP (1991).
27. B.N. Maker, R.M. Ferencz, J.O. Hallquist: "NIKE3D: A Nonlinear, Implicit, Three Dimensional Finite Element Code for Solid and Structural Mechanics - User's Manual, University of California, Lawrence Livermore National Laboratory, Report UCRL-MA-105268, January, 1991.

TABLE 1

FIBER AND MATRIX MATERIAL PROPERTIES

SCS-6 fiber properties

$\nu = 0.33$:

E = 413.7 GPa :

α (Secant CTE) = 4.86e-06

Titanium Aluminide (Ti-24Al-11Nb) At% matrix properties

Temp (°C)	Poisson Ratio	Elastic Modulus (GPa)	Plastic Modulus (GPa)	Yield Strength (GPa)	Secant CTE (10^{-6}/°C)
21	0.3	68.9	3.72	0.4990	12.15
149	0.3	67.6	4.21	0.4413	12.40
260	0.3	66.2	4.69	0.3902	12.69
427	0.3	64.8	5.38	0.3199	13.30
649	0.3	62.1	4.96	0.2599	14.85
760	0.3	51.0	2.48	0.2399	15.89
950	0.3	32.4	2.48	0.1103	18.72

Note: Reference [16]: T_{ref} = 900° C

Beta-21S matrix properties

Temp (°C)	Poisson Ratio	Elastic Modulus (GPa)	Plastic Modulus (GPa)	Yield Strength (GPa)	Secant CTE (10^{-6}/°C)
21	0.34	117	3.84	1.0500	9.940
316	0.34	101	5.40	0.7750	10.493
482	0.34	95.4	6.38	0.6900	10.824
566	0.34	78.1	16.96	0.4700	10.994
621	0.34	73.2	14.72	0.2890	11.108
650	0.34	70.6	0.0	0.2690	11.168
900	0.34	50.9	0.0	0.0940	11.685

Note: Reference [16]: T_{ref} = 900° C

Table 2. Two-ply Model

Average residual stresses (MPa) in Ti-24Al-11Nb Matrix Material

	As-Cooled Condition				After Removing Each Layer			
Layer Number/ Distance from fibers (microns)	$\langle\sigma\rangle_L$	$\langle\sigma\rangle_T$	$\langle\sigma\rangle_Z$	$\langle\sigma\rangle_E^*$	$\langle\sigma\rangle_L$	$\langle\sigma\rangle_T$	$\langle\sigma\rangle_Z$	$\langle\sigma\rangle_E^*$
(1) 70.00	298	93	0	256	298	93	0	258
(2) 61.25	298	96	-9	263	300	97	0	262
(3) 52.50	298	97	-17	270	305	99	-1	270
(4) 43.75	298	94	-33	283	311	102	-1	275
(5) 35.00	298	91	-51	298	315	107	0	277
(6) 26.25	298	87	-72	316	319	110	0	281
(7) 17.50	298	89	-99	338	328	111	0	289

Average residual stresses (MPa) in Beta-21S Matrix Material

	As-Cooled Condition				After Removing Each Layer			
Layer Number/ Distance from fibers (microns)	$\langle\sigma\rangle_L$	$\langle\sigma\rangle_T$	$\langle\sigma\rangle_Z$	$\langle\sigma\rangle_E^*$	$\langle\sigma\rangle_L$	$\langle\sigma\rangle_T$	$\langle\sigma\rangle_Z$	$\langle\sigma\rangle_E^*$
(1) 70.00	283	85	0	251	283	85	0	252
(2) 61.25	283	85	-3	254	289	89	-1	257
(3) 52.50	283	85	-10	259	296	94	1	261
(4) 43.75	283	85	-19	266	303	97	-1	269
(5) 35.00	283	85	-31	275	311	98	0	275
(6) 26.25	283	85	-44	285	319	100	0	283
(7) 17.50	283	85	-59	298	327	103	-1	290

*$\langle\sigma\rangle_E$ = Von Mises Effective Stress

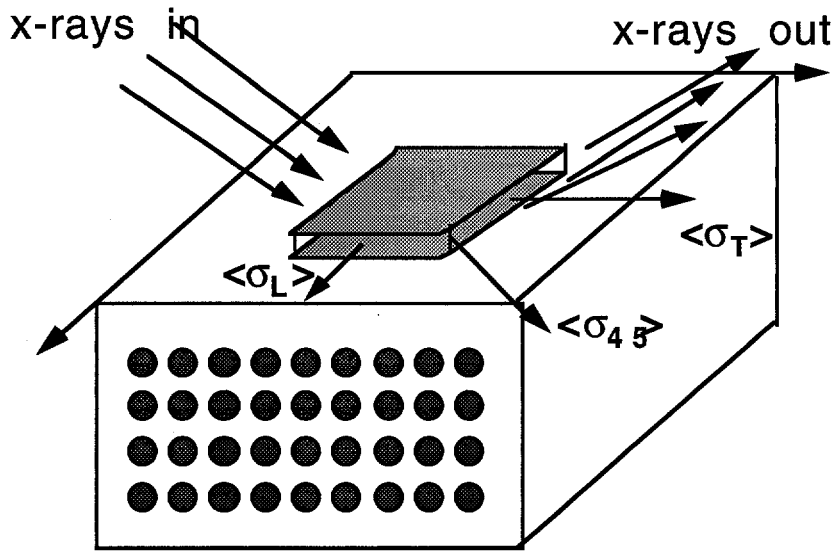

Figure 1- Schematic of a fiber reinforced MMC showing the directions of stress measurement and the region on the surface of the composite where the x-ray beam is sampled.

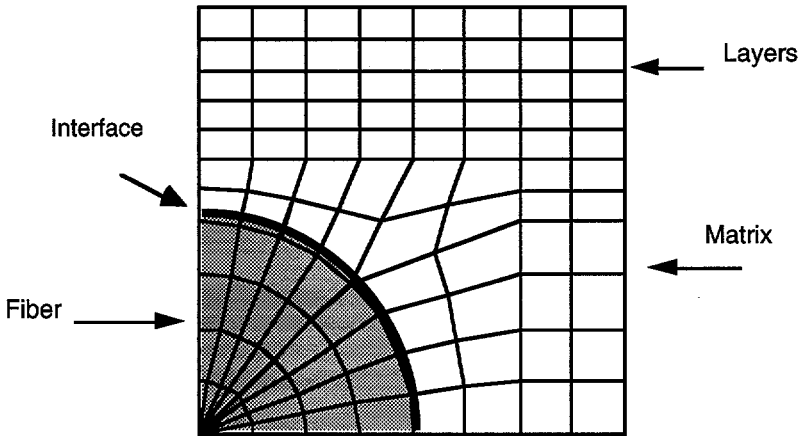

Figure 2 - A schematic of a one quarter fiber (1/4x1) model showing the arrangement of matrix material in the form of layers. In conventional terminology this is also known as **unit-cell finite element model**.

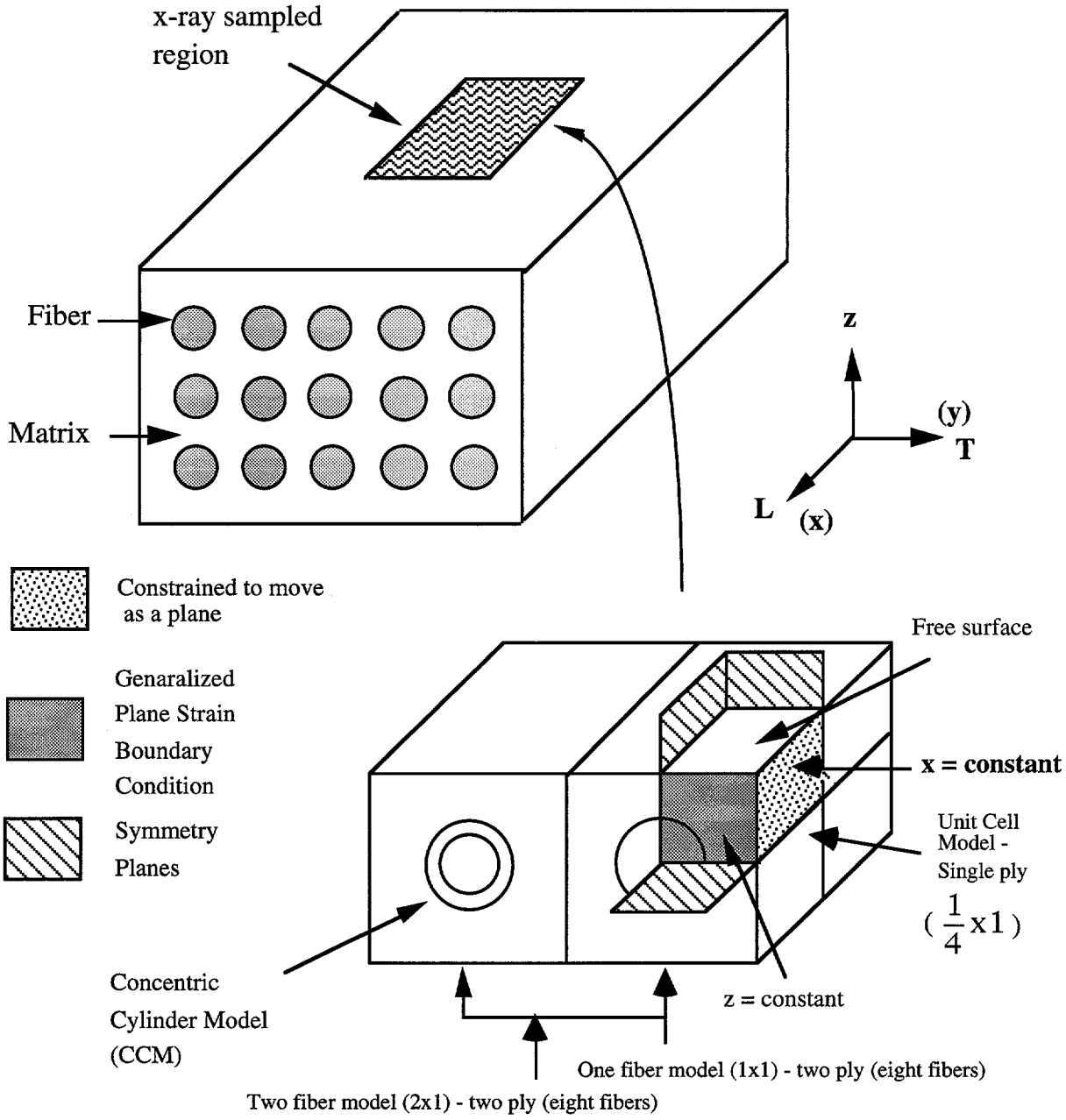

Figure 3 - Schematic representation of concentric cylinder and unit cell models of MMCs showing symmetry, generalized and constrained to move as a plane, boundary conditions. The extension of the unit cell model to a one and two fiber models is also shown.

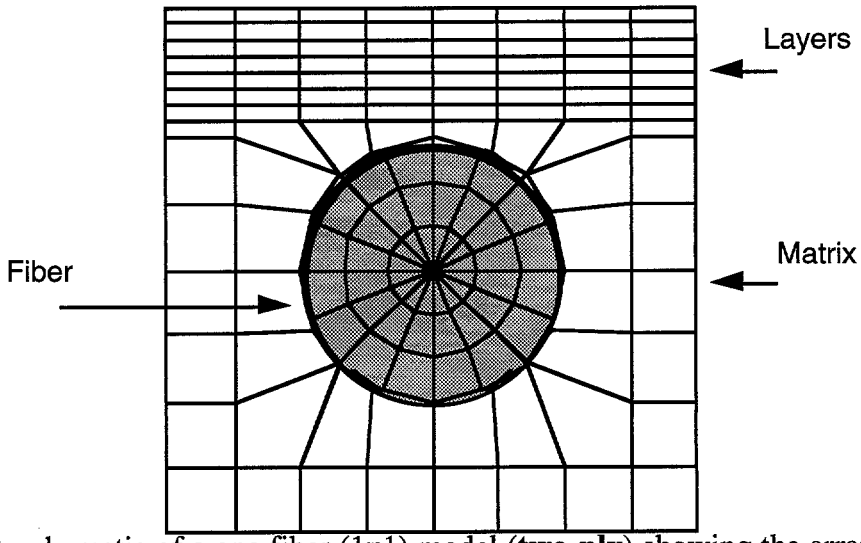

Figure 4 - A schematic of a one fiber (1x1) model (**two-ply**) showing the arrangement of matrix material in the form of layers.

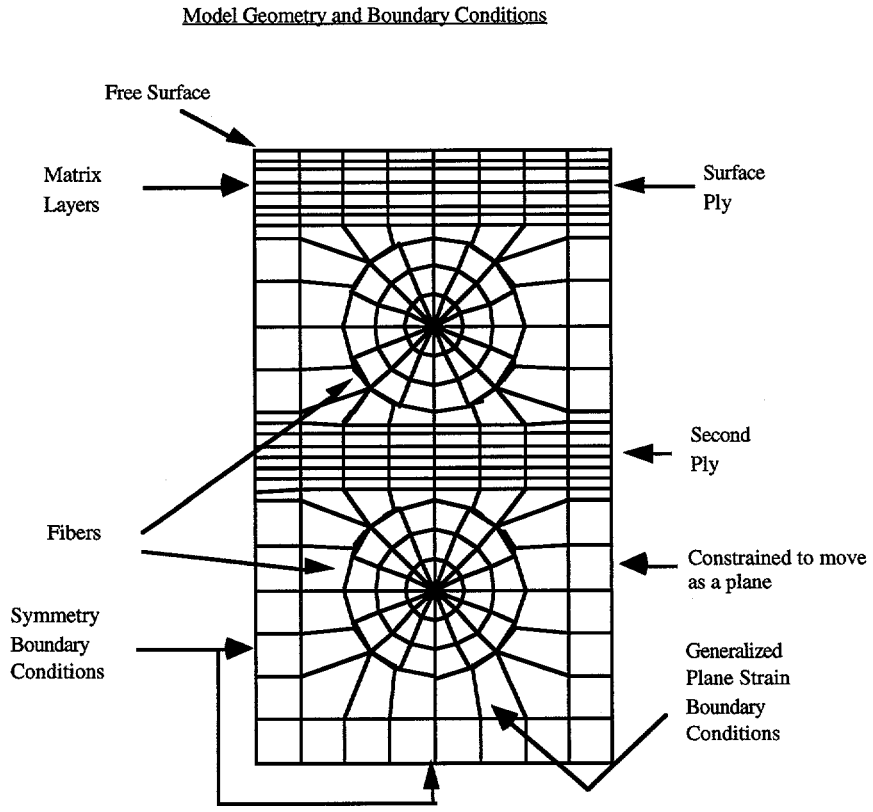

Figure 5 - A view of the **four-ply** (1x4) FEM model showing the matrix material in the surface and the second internal ply arranged in the form of layers.

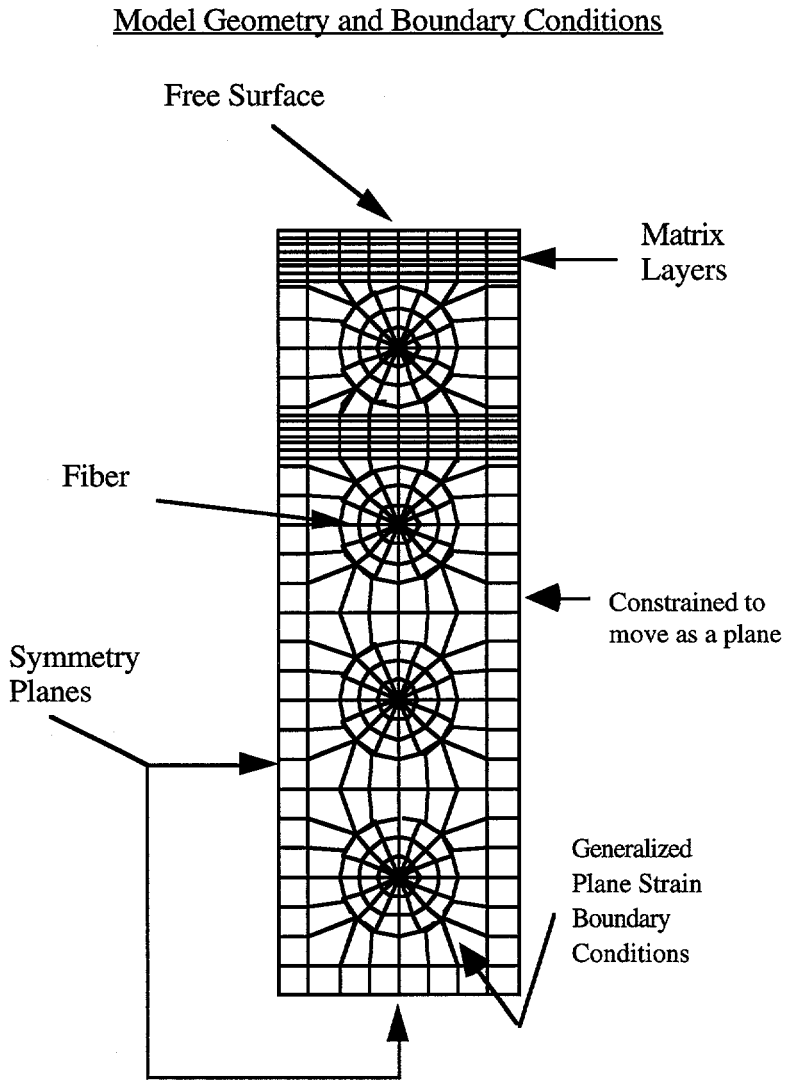

Figure 6 - A view of the **eight-ply** (1x8) FEM model showing the matrix material in the surface ply and the second internal ply arranged in the form of layers.

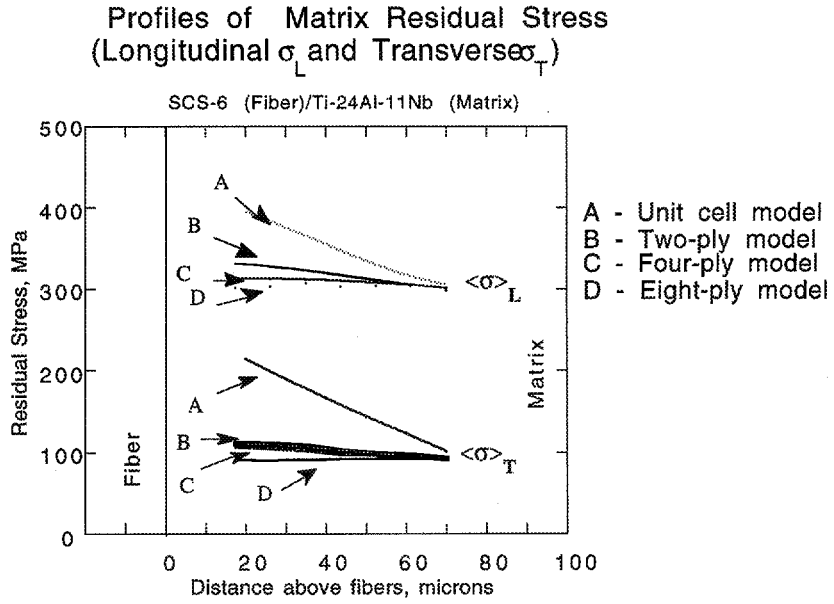

Figure 7 - Comparison of longitudinal and transverse residual stress profiles between finite element models [unit cell model, two-ply, four-ply and eight-ply]

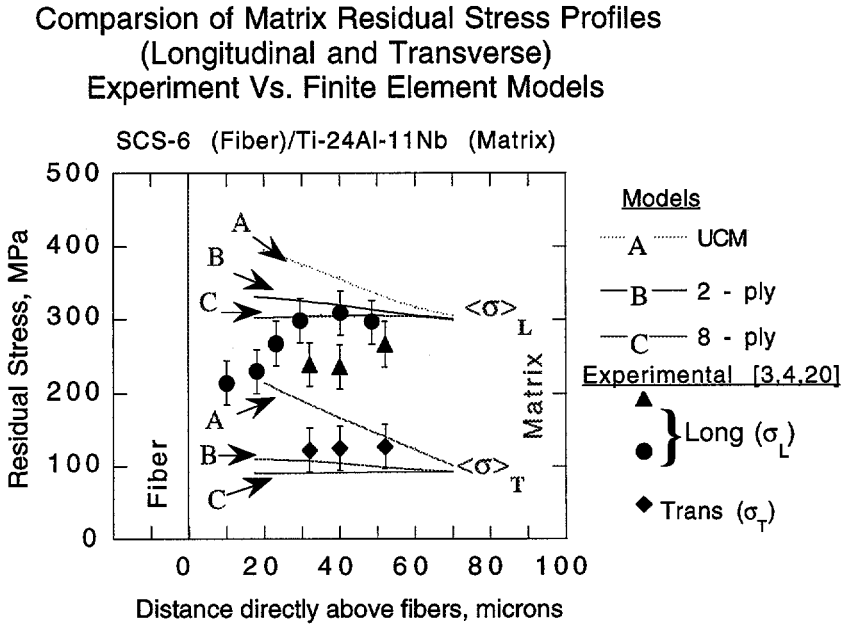

Figure 8 - Comparison of longitudinal and transverse residual stress profiles between finite element models [unit cell model, two-ply and eight-ply] and experimental results.

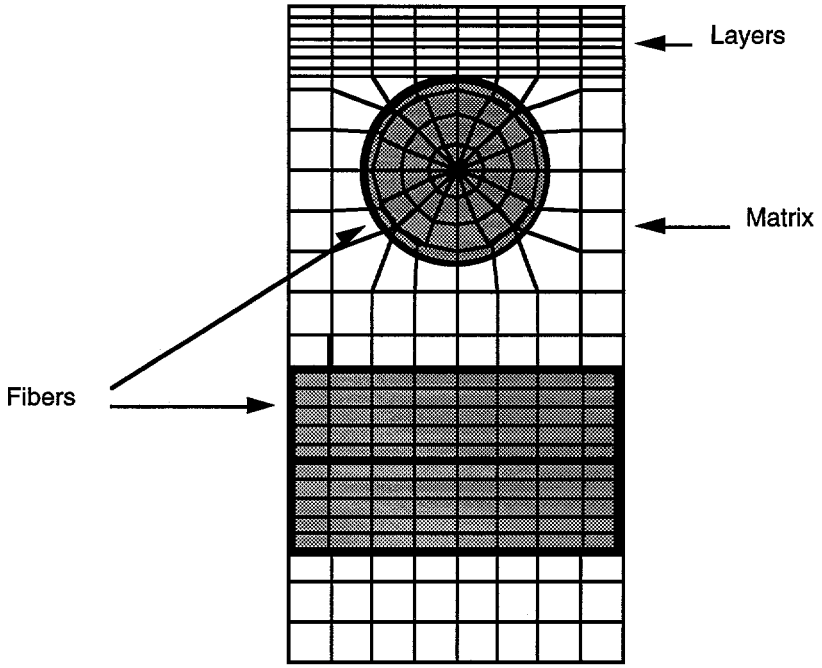

Figure 9 - Schematic of a cross-ply [0/90] model showing the arrangement of matrix material in the form of layers.

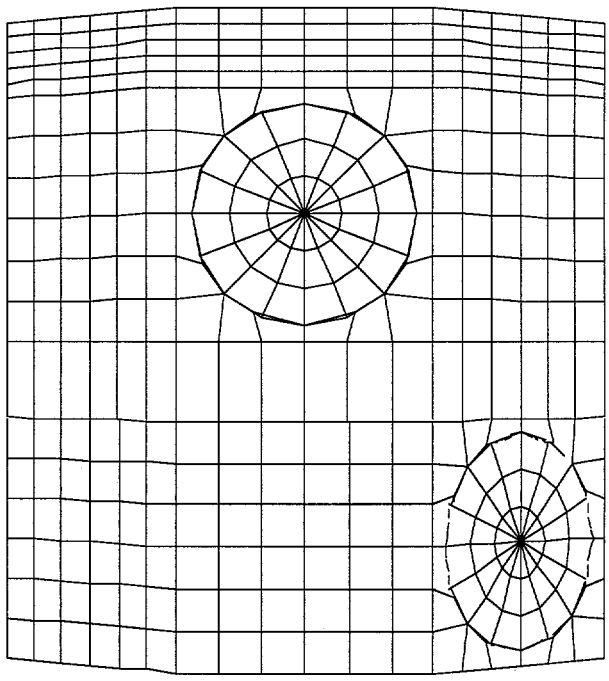

Figure 10 - A view of the $[0/45]_s$ model showing the arrangement of the matrix material in the form of layers.

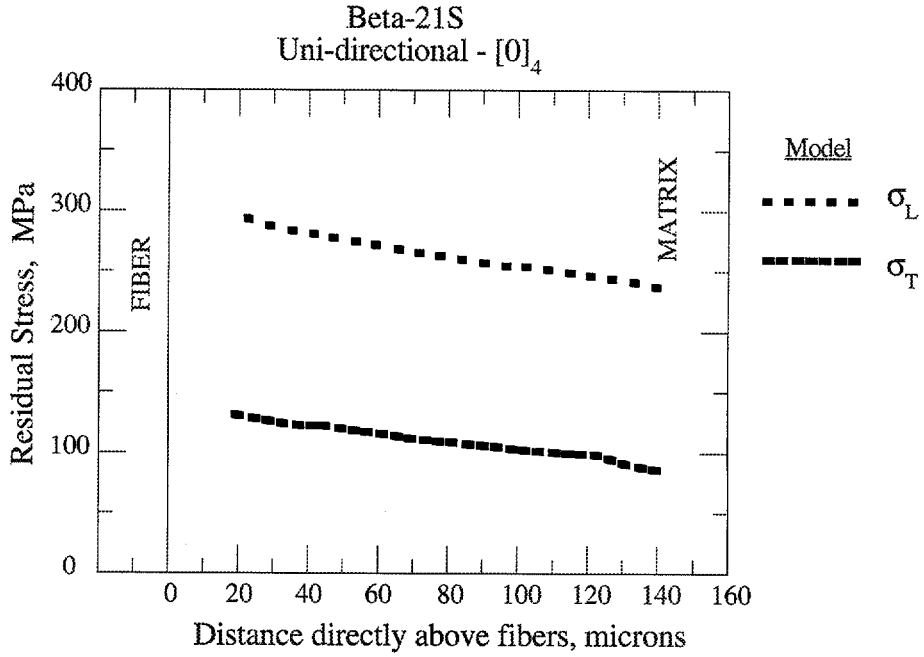

(A)

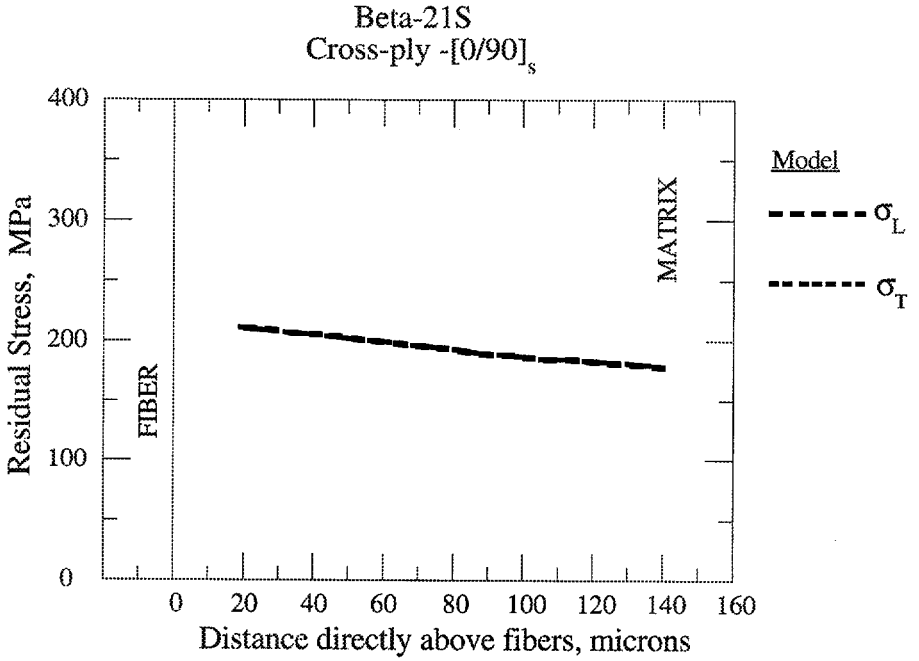

(B)

Figure 11 - Comparison of matrix longitudinal and transverse residual stress profiles for the **(A)** $[0]_4$ (four-ply) and **(B)** $[0/90]_s$ (cross-ply), finite element models in the as-received condition.

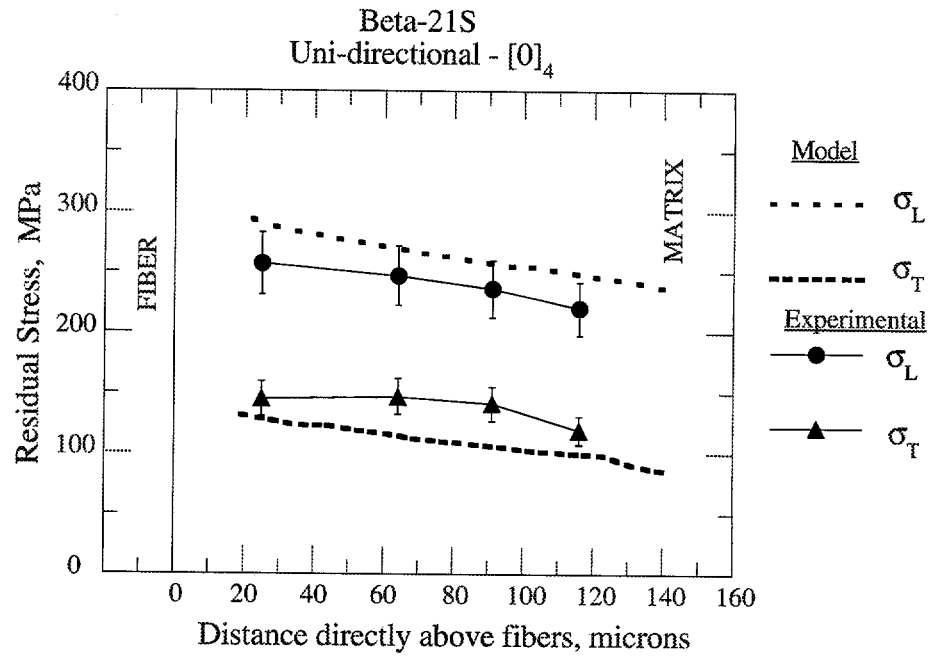

(A)

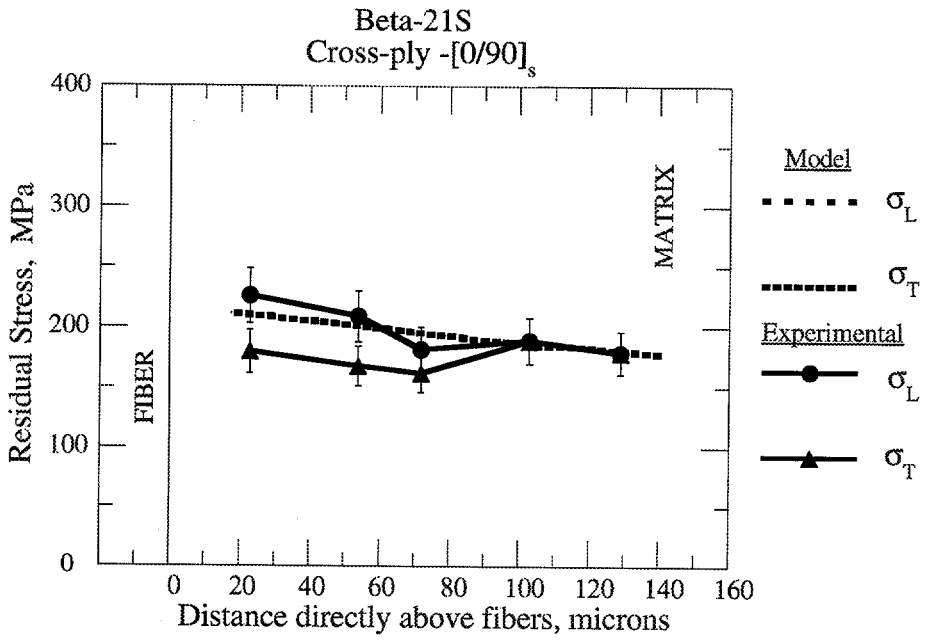

(B)

Figure 12 - Comparison of matrix longitudinal and transverse residual stress profiles between **(A)** $[0]_4$ **(four-ply)** and **(B)** $[0/90]_s$ **(cross-ply)**, finite element models and experimental results,

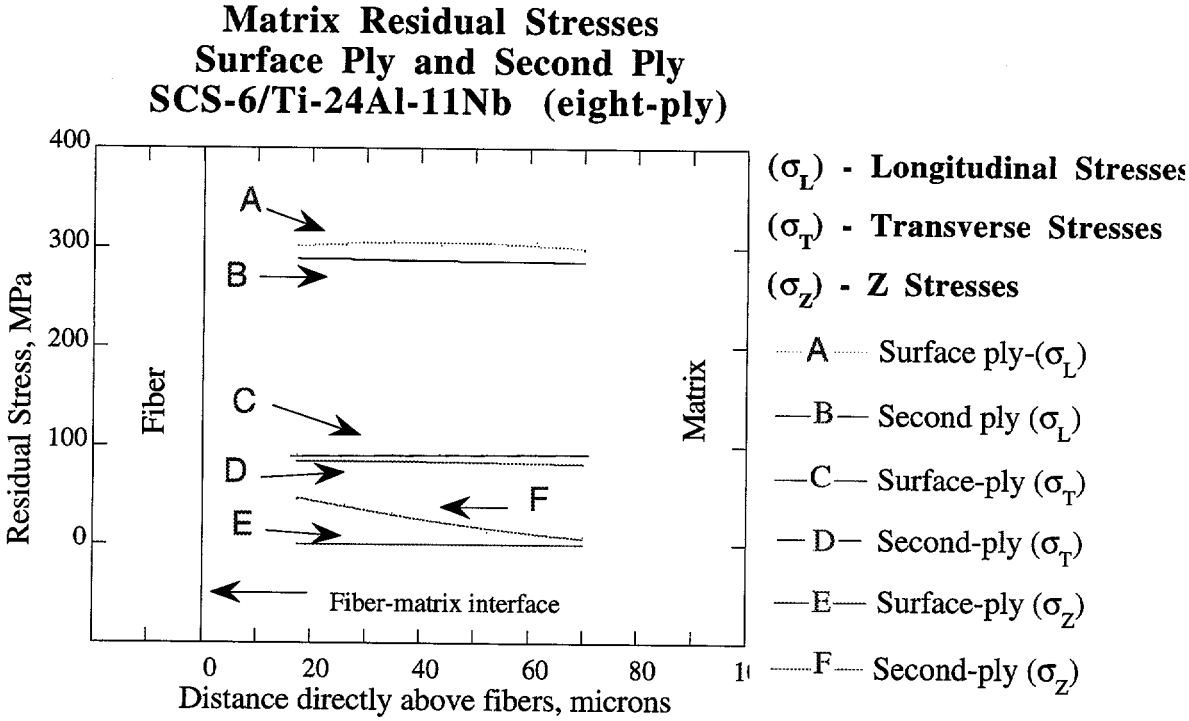

Figure 13 - Comparison of matrix longitudinal (σ_L), transverse (σ_T), and out-of-plane (σ_Z) profiles between surface ply and second ply for the eight-ply $[0]_8$ uni-directional composite.

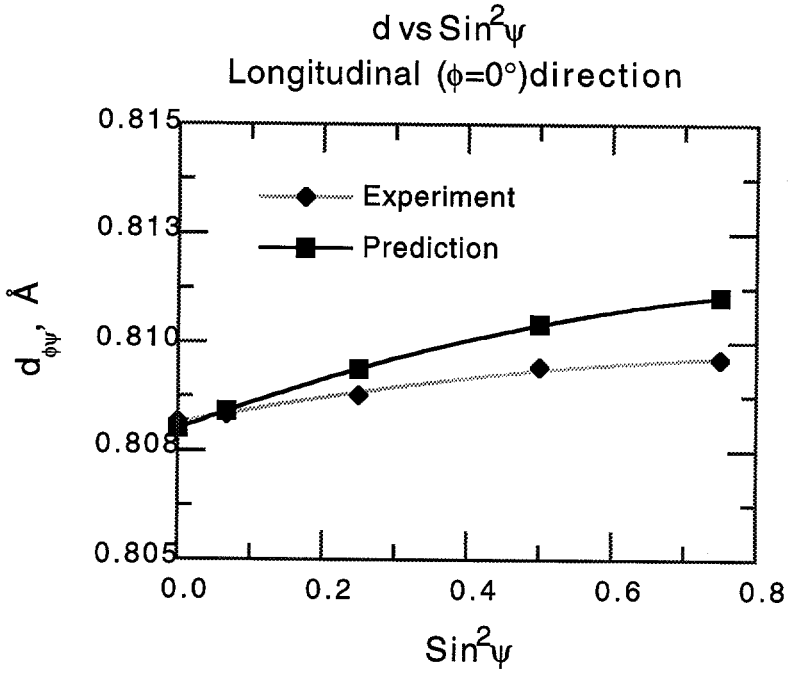

(A)

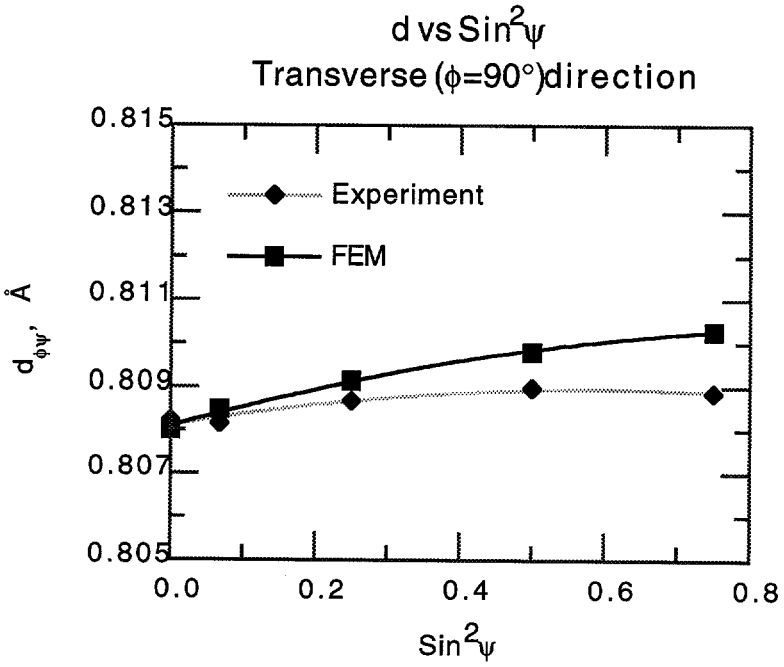

(B)

Figure 14 - Comparison of d vs. $Sin^2\psi$ plots for the (A) longitudinal and(B) transverse directions between experimental results and predictions from FEM models in the second ply region for a SCS-6/Ti-24Al-11Nb MMC.